Available online at www.sciencedirect.com
ScienceDirect
Journal of Sound and Vibration 324 (2009) 690–711
JOURNAL OF SOUND AND VIBRATION
www.elsevier.com/locate/jsvi

Calibration of the damping dispersion parameter in a non-parametric probabilistic approach

B. Goller, M.F. Pellissetti*

Institute of Engineering Mechanics, University of Innsbruck, Technikerstr. 13, A-6020 Innsbruck, Austria

Received 6 March 2008; received in revised form 16 February 2009; accepted 17 February 2009
Handling Editor: C.L. Morfey
Available online 8 April 2009

Abstract

Response predictions in structural dynamics are in general very sensitive to random uncertainties associated with the underlying predictive mathematical model. One way to capture parametric and model uncertainties consists in the construction of a non-parametric probabilistic model, in which the reduced structural matrices are replaced by random matrices. The uncertainties are introduced at a global level and controlled through one dispersion parameter each, for the mass, damping and stiffness matrix.

In the present paper the role of the damping dispersion parameter is investigated, for the case in which the adopted non-parametric model is calibrated with respect to an existing parametric model. It is shown that in the non-parametric model the influence of the damping dispersion on the scatter in the frequency response is relatively small, if a calibration criterion based on matrix norms is used.

A novel method for calibrating this non-parametric model is proposed, which enforces the same scatter of the frequency response function (FRF) at the first resonance frequency, in the parametric and the non-parametric model. A case study involving a satellite FE model shows that with this approach the FRF scatter of the non-parametric model reaches a level similar to that of the parametric model used for its calibration.

1. Introduction

The use of mathematical models of structures for the purpose of response predictions is always associated with unavoidable, inherent uncertainties. Probabilistic models are a suitable means to capture random uncertainties and to enhance the predictive quality. Such improvements are of great relevance for numerous fields of engineering, such as aerospace engineering.

The uncertainties associated with the numerical model can be classified into *parameter uncertainties* and *model uncertainties* [1]. The former relate to the parameters of the mathematical model; more specifically to material parameters, such as the elasticity modulus or the mass density, and to geometrical parameters, such as the cross-section dimensions of structural members. The random character attributed to the parameters of

*Corresponding author. Tel.: +43 512 507 6841; fax: +43 512 507 2905.
E-mail addresses: mechanik@uibk.ac.at, manuel.pellissetti@uibk.ac.at (M.F. Pellissetti).
URL: http://mechanik.uibk.ac.at (M.F. Pellissetti).

0022-460X/$ - see front matter © 2009 Elsevier Ltd. All rights reserved.
doi:10.1016/j.jsv.2009.02.039

the mathematical model is meant to mimic the scatter which is observed when these parameters are measured (directly or indirectly) for each specimen of a set of samples. This scatter is in turn due to the variability in the manufacturing conditions and processes and the inherent variability of the material micro-structure. The uncertainty affecting these parameters can be accounted for by modelling these as random quantities, i.e. by constructing a so-called parametric model of uncertainties (see e.g. Refs. [2–5]). Probability theory is not the only tool for modelling this variability, but it is adequate in numerous situations of engineering interest.

The one-of-a-kind, actual, physical structure which is realized and utilized in reality, such as the satellite considered in this manuscript, is then viewed as a single realization. Clearly, the values of its parameters are fixed for this one structure, however, they are unknown due to the lack of control over the above mentioned causes of variability. With this parametric approach, the uncertainty associated with each of the parameters of the model is accounted for *explicitly*. The uncertainty can thus be captured locally, down to a level corresponding to the degree of resolution of the mathematical model.

Uncertainties, which have their origin at a level lower than the current degree of resolution, are often referred to as *model uncertainties* [6,7,1]. They are hence related to the simplifications introduced in the modelling process with the goal of decreasing the complexity of the model. Model uncertainties in structural dynamics are currently receiving considerable attention, as documented by the execution of a recent benchmark study organized by Sandia National Laboratories [8].

The non-parametric model of uncertainties introduced by Soize [9–11] has been proposed for structural dynamics problems, in order to capture model uncertainties in addition to the parametric uncertainties. In this non-parametric model, the uncertainties are introduced at a *global level*, using the reduced nominal numerical model. The latter is obtained with the truncated modal basis of the full nominal model.

In context of an earlier study it has been observed [12] that responses obtained with this approach exhibit a very low sensitivity of the predicted frequency response functions (FRF) to damping uncertainty, especially for excitations in the low frequency range. This is a clearly distinct feature of the adopted non-parametric model, compared to the parametric model, in which the damping parameters strongly influence the frequency response. In particular, a significantly different sensitivity with respect to scatter in the damping has been observed even if (i) the same mathematical model is used to construct the parametric and the used non-parametric model, and (ii) the adopted non-parametric model is calibrated on the basis of the parametric model [13].

The first objective of this paper is to quantitatively analyse the influence of damping uncertainty on the frequency response in the adopted non-parametric and parametric approach in the context of two numerical examples. For this purpose, first the effect of changing the damping dispersion level in the non-parametric model is investigated, under the assumption of both deterministic and random mass and stiffness matrices (Sections 3.2 and 4.2). This effect is also analysed in models with comparatively high nominal damping (Section 4.3). Following the observation that the effect of scatter in the damping is significantly smaller in the non-parametric model, compared to the underlying parametric model, a detailed analysis of the scatter in the damping matrix entries, both in the parametric and the non-parametric model (Section 4.5), has been performed.

The second objective of the paper consists in the development of a novel calibration procedure for the damping dispersion parameter. In earlier publications the latter is controlled using a procedure which enforces the agreement of the scatter magnitude of the damping matrices of the parametric and the non-parametric model [14].

Recently, a methodology has been introduced for the estimation of the dispersion parameters on the basis of experimental measurements of the frequency domain transfer functions. Thus far, the application of the methodology has been performed under the simplifying assumption that all three dispersion parameters are identical [15]. In this manuscript, an alternative procedure is proposed, with the aim of introducing the same sensitivity of the frequency response to the dispersion of the damping, both in the non-parametric model and the parametric model used for its calibration, with the main objective to obtain a better agreement of the non-parametric and the underlying parametric model of uncertainties.

The investigations related to the above two objectives are performed in the context of two case studies, namely a simply supported beam and a more complex satellite structural model.

2. Method of analysis

2.1. Mathematical model

The mathematical model considered in this paper corresponds to a time-invariant damped dynamical system, discretized with the finite element method. The resulting force excited, multi-degree-of-freedom system is governed by the equation of motion, which for a harmonic excitation with angular frequency ω leads to the following matrix equation:

$$(-\omega^2 \underline{\mathbf{M}} + \mathrm{i}\omega \underline{\mathbf{D}} + \underline{\mathbf{K}})\,\underline{\mathbf{u}}(\omega) = \underline{\mathbf{f}}(\omega), \tag{1}$$

where $\underline{\mathbf{M}}$, $\underline{\mathbf{D}}$ and $\underline{\mathbf{K}}$ are the deterministic, symmetric and positive-semidefinite structural mass, damping, and stiffness matrices, respectively. Furthermore, $\underline{\mathbf{f}}(\omega)$ is the force vector at each frequency ω within the considered frequency band $[\omega_{\min}, \omega_{\max}]$, and $\underline{\mathbf{u}}(\omega)$ represents the vector of the complex displacements of each degree of freedom (DOF), induced by the external force vector $\underline{\mathbf{f}}(\omega)$.

2.2. Parametric probabilistic approach

In the parametric probabilistic approach, the parameters of the mathematical model are modelled as random variables. Consequently, the structural matrices in Eq. (1) can be viewed as functions of the set of random parameters $\{X_i\}_{i=1}^{L}$. The latter can be collected in a random vector $\mathbf{X} = \mathbf{X}(\theta)$, where θ denotes a sample in the sample space $\mathscr{S}$ and thus indicates the random nature of $\mathbf{X}$. Hence, the deterministic matrices in Eq. (1) are replaced by the random matrices $\mathbf{M}^{\mathrm{par}}(\mathbf{X}), \mathbf{D}^{\mathrm{par}}(\mathbf{X}), \mathbf{K}^{\mathrm{par}}(\mathbf{X})$, where "par" stands for "parametric model".

For large systems the matrix equation corresponding to Eq. (1) can be computed efficiently with a reduced version of the equation,

$$(-\omega^2 \mathbf{M}_{\mathrm{red}}^{\mathrm{par}} + \mathrm{i}\omega \mathbf{D}_{\mathrm{red}}^{\mathrm{par}} + \mathbf{K}_{\mathrm{red}}^{\mathrm{par}})\mathbf{Q}^{\mathrm{par}}(\omega) = \mathscr{F}(\omega), \tag{2}$$

in which $\mathscr{F}(\omega) = \mathbf{\Phi}^{\mathrm{T}}\,\underline{\mathbf{f}}(\omega)$ and $\mathbf{M}_{\mathrm{red}}^{\mathrm{par}}$, $\mathbf{D}_{\mathrm{red}}^{\mathrm{par}}$ and $\mathbf{K}_{\mathrm{red}}^{\mathrm{par}}$ are the diagonal, random, reduced mass, damping and stiffness matrices $(n \times n)$,

$$\mathbf{M}_{\mathrm{red}}^{\mathrm{par}} = \mathbf{\Phi}^{\mathrm{T}}\mathbf{M}^{\mathrm{par}}\mathbf{\Phi}, \quad \mathbf{D}_{\mathrm{red}}^{\mathrm{par}} = \mathbf{\Phi}^{\mathrm{T}}\mathbf{D}^{\mathrm{par}}\mathbf{\Phi}, \quad \mathbf{K}_{\mathrm{red}}^{\mathrm{par}} = \mathbf{\Phi}^{\mathrm{T}}\mathbf{K}^{\mathrm{par}}\mathbf{\Phi}. \tag{3}$$

In the above equation, $\mathbf{\Phi}$ is an $(m \times n)$ real matrix whose columns are the $n \lll m$ eigenvectors $\mathbf{\Phi}_\alpha$ related to the n lowest, strictly positive eigenvalues $\Lambda_\alpha = \omega_\alpha^2$, corresponding to the generalized eigenvalue problem,

$$\mathbf{K}^{\mathrm{par}}\mathbf{\Phi}_\alpha = \Lambda_\alpha \mathbf{M}^{\mathrm{par}}\mathbf{\Phi}_\alpha. \tag{4}$$

It should be noted that the diagonal character of the damping matrix is only true if the n modes that are included in the model have classical damping, i.e. if the unreduced structural model has a damping matrix satisfying the Caughey commutativity condition.

In the above equations (2)–(4), the quantities $\mathbf{\Phi}$, $\mathbf{\Lambda}$, $\mathbf{M}_{\mathrm{red}}^{\mathrm{par}}$, $\mathbf{D}_{\mathrm{red}}^{\mathrm{par}}$, $\mathbf{K}_{\mathrm{red}}^{\mathrm{par}}$ are functions of $\mathbf{X}$, since they depend on $\mathbf{M}^{\mathrm{par}}(\mathbf{X})$, $\mathbf{D}^{\mathrm{par}}(\mathbf{X})$ and $\mathbf{K}^{\mathrm{par}}(\mathbf{X})$. Therefore, also the solution vector of Eq. (2) is a function of $\mathbf{X}$, i.e. $\mathbf{Q}^{\mathrm{par}}(\mathbf{X}, \omega)$. In contrast, the excitation is assumed to be deterministic, i.e. in the sequel the uncertainty is assumed to be limited to the mass, stiffness and damping matrices.

Upon solution of Eq. (2) for $\mathbf{Q}^{\mathrm{par}}(\mathbf{X}, \omega)$, the $\mathbb{C}^m$-valued random vector $\mathbf{U}^{\mathrm{par}}(\mathbf{X}, \omega)$ is reconstructed with the corresponding modal basis

$$\mathbf{U}^{\mathrm{par}}(\mathbf{X}, \omega) = \mathbf{\Phi}(\mathbf{X})\mathbf{Q}^{\mathrm{par}}(\mathbf{X}, \omega). \tag{5}$$

2.3. Non-parametric probabilistic approach

As mentioned in the Introduction, the non-parametric probabilistic model is an approach in which the uncertainty associated with the mass, damping and stiffness matrices is introduced globally. The approach

leads directly to a random matrix equation in the modal subspace

$$(-\omega^2\mathbf{M}_{\mathrm{red}}^{\mathrm{np}}(\delta_M) + \mathrm{i}\omega\mathbf{D}_{\mathrm{red}}^{\mathrm{np}}(\delta_D) + \mathbf{K}_{\mathrm{red}}^{\mathrm{np}}(\delta_K))\mathbf{Q}^{\mathrm{np}}(\omega) = \mathscr{F}(\omega), \tag{6}$$

where "np" stands for "non-parametric model".

Unlike the system matrices in Eq. (2), the matrices $\mathbf{M}_{\mathrm{red}}^{\mathrm{np}}$, $\mathbf{K}_{\mathrm{red}}^{\mathrm{np}}$ and $\mathbf{D}_{\mathrm{red}}^{\mathrm{np}}$ in the above equation are *full* matrices and are based on a particular probability model described in detail in Refs. [9–11]. The magnitude of the scatter of the elements of these matrices is governed globally by a so-called *dispersion parameter* for each of the matrices, i.e. by the parameters δ_M, δ_D and δ_K. Consequently, this approach is very different from the parametric model of uncertainties, in which the uncertainties are modelled locally and then propagated to the matrices in the modal subspace in Eq. (2), through the solution of the eigenvalue problem in Eq. (4) and the modal reduction in Eq. (3).

Upon solution of Eq. (6) for $\mathbf{Q}^{\mathrm{np}}(\omega)$, the $\mathbb{C}^m$-valued random vector $\mathbf{U}^{\mathrm{np}}(\omega)$ is reconstructed with the modal basis of the nominal numerical model, denoted by the underline,

$$\mathbf{U}^{\mathrm{np}}(\omega) = \underline{\mathbf{\Phi}}\,\mathbf{Q}^{\mathrm{np}}(\omega). \tag{7}$$

2.4. Calibration of the damping dispersion parameter

The identification of the damping dispersion parameter, δ_D, introduced in the previous section, can be carried out using different methods (see Ref. [16]). In the following analysis, the calibration with respect to a given parametric probabilistic model is discussed.

The calibration method adopted in Ref. [13] is based on the following expression:

$$\delta_D = \sqrt{\frac{W_D^{\mathrm{par}}(n+1)}{\mathrm{tr}(\underline{\mathbf{D}}_{\mathrm{red}})^2 + \mathrm{tr}(\underline{\mathbf{D}}_{\mathrm{red}}^2)}}, \tag{8}$$

where $\underline{\mathbf{D}}_{\mathrm{red}}$ denotes the nominal damping matrix in reduced form, n is the dimension of the reduced system and in which W_D^{par} is given by

$$W_D^{\mathrm{par}} = E\{\|\mathbf{D}_{\mathrm{red}}^{\mathrm{par}} - \underline{\mathbf{D}}_{\mathrm{red}}\|_F^2\}, \tag{9}$$

where $\|\mathbf{A}\|_F^2 = \mathrm{tr}(\mathbf{A}\mathbf{A}^{\mathrm{T}})$.

As shown in two cases studies discussed in depth in the next sections, this identification leads to a damping dispersion parameter that induces a scatter in the frequency response which is significantly smaller than the scatter in the *corresponding* parametric model. In view of this fact, an alternative calibration method is now introduced which tunes the dispersion parameter by comparing the scatter magnitude of the response, i.e. the output, rather than that of the damping matrices, i.e. the input.

FRF-peak-based calibration of the damping dispersion parameter. The main idea underlying this novel calibration procedure is the requirement that at the first eigenfrequency the scatter in the FRF of the non-parametric model converges to that of the parametric model, where convergence is measured in terms of the (approximate) PDF. The reasoning underlying this choice for the calibration criterion of the damping dispersion parameter δ_D is closely related to the argument for calibrating the dispersion parameters of the mass and the stiffness, δ_M and δ_K, by enforcing the same scatter in the first eigenfrequency, for both the parametric and the non-parametric model [13]. More specifically, this reasoning is based on the observation that in structural dynamics numerical models are generally constructed such that the model is particularly robust with respect to model uncertainties around the first eigenfrequency.

In the following it is assumed that in the process of the calibration of the damping dispersion parameter, the scatter of the mass and stiffness properties is neglected, both for the parametric and the non-parametric model.

Let the frequency responses of the quantity of interest, due to a harmonic excitation at the first eigenfrequency ω_1, expressed by the vector $\underline{\mathbf{f}}(\omega_1)$, be denoted by Y_1^{par} and Y_1^{np} for the parametric model and the non-parametric model, respectively. The corresponding probability density functions (PDFs) of the responses are denoted by $p_{Y_1^{\mathrm{par}}}$ and $p_{Y_1^{\mathrm{np}}}$, respectively. It should be noted that $p_{Y_1^{\mathrm{par}}}$ clearly depends on the uncertainty model adopted for the damping parameters in the parametric probabilistic model.

The functional $J(\delta_D)$ is then introduced as a measure of the difference between the two PDFs,

$$J(\delta_D) = \frac{\| p_{Y_1^{\mathrm{np}}}(\delta_D) - p_{Y_1^{\mathrm{par}}} \|_{\mathscr{L}^2}}{\| p_{Y_1^{\mathrm{par}}} \|_{\mathscr{L}^2}}, \tag{10}$$

where the norm $\|f\|_{\mathscr{L}^2}$ is given by

$$\|f\|_{\mathscr{L}^2} = \left(\int_{\mathbb{R}} |f(x)|^2 \, \mathrm{d}x \right)^{1/2}. \tag{11}$$

In Eq. (10) the dependence of the PDF of Y_1^{np}, $p_{Y_1^{\mathrm{np}}}$, on the dispersion parameter δ_D is made explicit.

The identification of the damping dispersion parameter δ_D is then carried out by solving the following minimization problem:

$$\delta_D = \arg\min J(\delta_D), \quad 0 \leqslant \delta_D \leqslant \sqrt{\frac{n_0 + 1}{n_0 + 5}}, \tag{12}$$

where n_0 is an integer less than or equal the dimension of the structural matrices, cf. Ref. [11].

Using Eqs. (10)–(12) for determining δ_D means that the dispersion parameter δ_D is tuned until the PDF of the frequency response of the non-parametric model converges to that of the parametric model.

It should be noted that the minimization of the L_2-norm of the differences of the two PDFs cannot enforce agreement of the tails of the distributions. However, this is of secondary importance in the present manuscript, since the analysis of low-probability events, i.e. reliability analysis, is not within the scope of the present paper.

3. Case study—beam model

3.1. Deterministic FE model

As a first example a beam model (see Ref. [15]) has been chosen for the analysis of the influence of the damping dispersion parameter on the scatter of the FRFs obtained with the non-parametric probabilistic approach. The simply supported, elastic beam shown in Fig. 1 has a length of 10 m and the dimensions of the cross section are 1.0×1.5 m. The excitation consists in a point load on the top surface in z-direction and the response quantity of interest consists in the acceleration of the node indicated in Fig. 1 in the same direction.

The normal mode analysis of the nominal FE model is performed using the commercial FE code MSC.Nastran [17]. The resulting eigenvalues and eigenmodes of the structure are then imported into MATLAB [18], for the analysis with both the non-parametric and the parametric model, respectively.

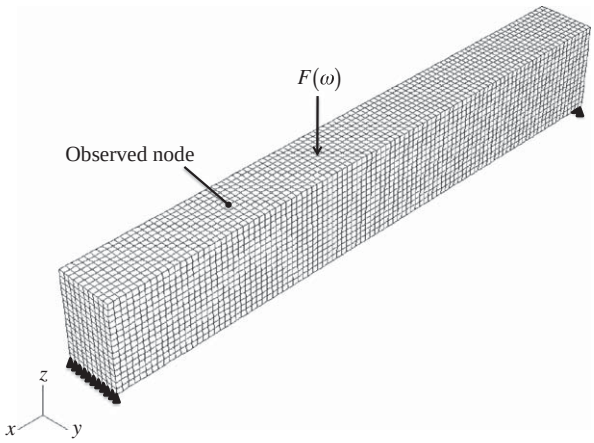

Fig. 1. Finite element model of the beam [15].

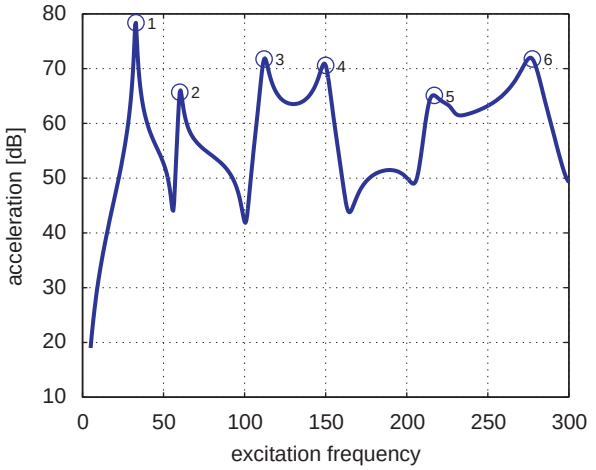

Fig. 2. Nominal structural response with numeration of peaks used for the following analysis.

Damping model. In the present model, dissipation is modelled exclusively through modal damping, i.e. the damping matrix of the mean reduced model, $\mathbf{D}_{\text{red}}^{\text{par}}$ in Eq. (2) is diagonal and the diagonal entries are of the form

$$\mathbf{D}_{\text{red}\,\alpha\alpha}^{\text{par}} = 2\omega_\alpha \xi_\alpha, \tag{13}$$

where ω_α and ξ_α are the α-th eigenfrequency and modal damping ratio, respectively. In the nominal model, the modal damping ratios have been assumed to take a constant value of $\xi_\alpha = 0.02$ for all modes. The frequency response of the nominal model is depicted in Fig. 2; the most prominent peaks are circled and labelled, as they will be referred to in the following analysis.

3.2. Influence of the damping dispersion on the frequency response scatter

In order to analyse the influence of the level of damping dispersion on the FRF scatter only uncertainties of the damping matrix are taken into account and the mass and the stiffness matrix are modelled with their mean (deterministic) values. A coefficient of variation (ratio of standard deviation over mean) of 20% is used for the reference parametric damping matrix which leads to a non-parametric damping matrix characterized by a damping dispersion parameter equal to $\delta_D = 0.22$, if the calibration criterion based on the agreement of the damping matrix norm (see Eq. (8)) is used.

The probabilistic analysis of the FRF has been carried out both for the reference parametric model and the corresponding non-parametric model, using Monte Carlo simulation. A convergence analysis has been carried out in order to determine the necessary number of Monte Carlo simulations for obtaining reliable estimates of the quantiles. The convergence analysis has been performed with respect to the FRF quantiles at the peaks indicated in Fig. 2; the convergence of the quantiles at the first peak is shown in Fig. 3. Based on the convergence analysis, a number of 1000 simulations is considered sufficient for the subsequent analysis of the 1%- and 99%-quantiles of the FRF peaks.

The confidence regions defined by the 1%- and 99%-quantiles of the acceleration due to an excitation in the range of [5,300] Hz are shown both for the parametric approach (see Fig. 4) and for the non-parametric approach (see Fig. 5). These two figures qualitatively show a significant difference in the magnitude of the scatter around the peaks between the two approaches.

A quantitative comparison of the scatter of the FRF peaks is shown in Fig. 6, where the confidence regions are delimited by the 1%- and 99%-quantiles, and in Fig. 7, where the confidence region delimited by the mean values plus/minus one standard deviation is shown for each of the seven peaks marked in Fig. 2. In addition, Table 1 lists the values of the standard deviations of the FRF peaks. The standard deviations of the FRF

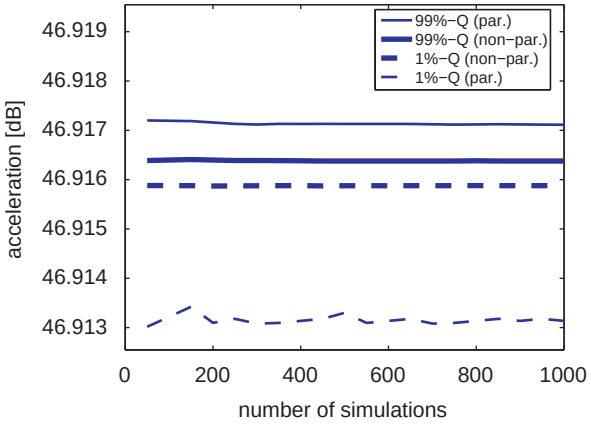

Fig. 3. Convergence analysis of the 1%- and 99%-quantiles of the second FRF peak obtained with the parametric ($\mathrm{CoV}_D = 0.20$) and non-parametric approach ($\delta_D = 0.22$); mass and stiffness deterministic.

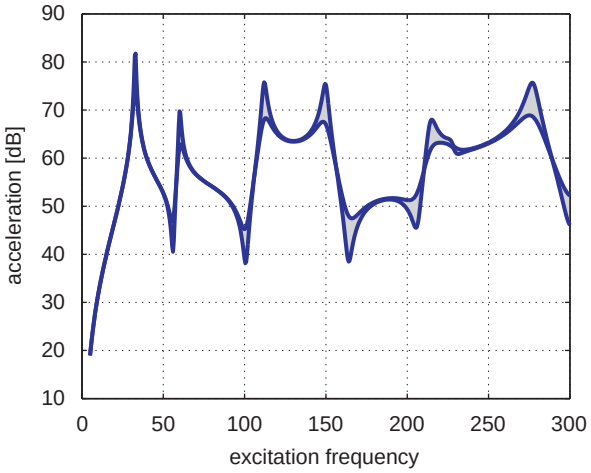

Fig. 4. Confidence region of the FRF delimited by the 1%- and 99%-quantiles, parametric approach; mass and stiffness deterministic ($\mathrm{CoV}_M = \mathrm{CoV}_K = 0.0$).

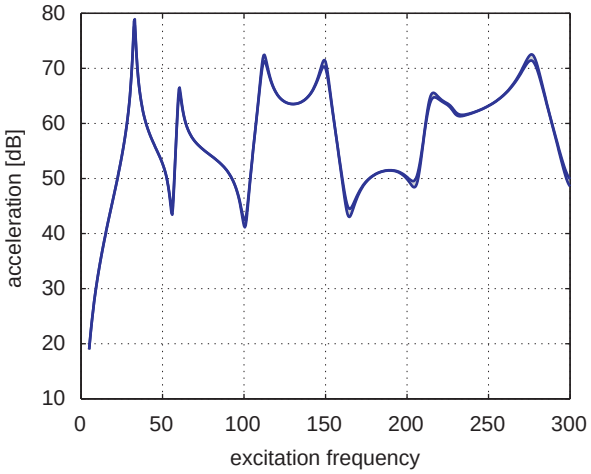

Fig. 5. Confidence region of the FRF delimited by the 1%- and 99%-quantiles, non-parametric approach; mass and stiffness deterministic ($\delta_M = \delta_K = 0.0$).

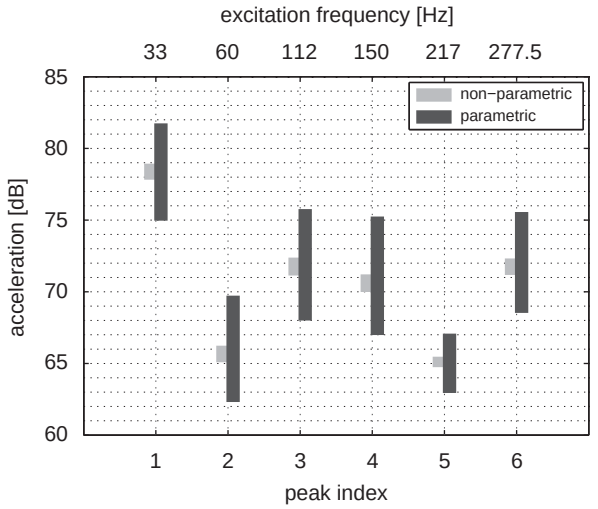

Fig. 6. Confidence region of the FRF peaks delimited by the 1%- and 99%-quantiles, parametric and non-parametric approach; mass and stiffness deterministic.

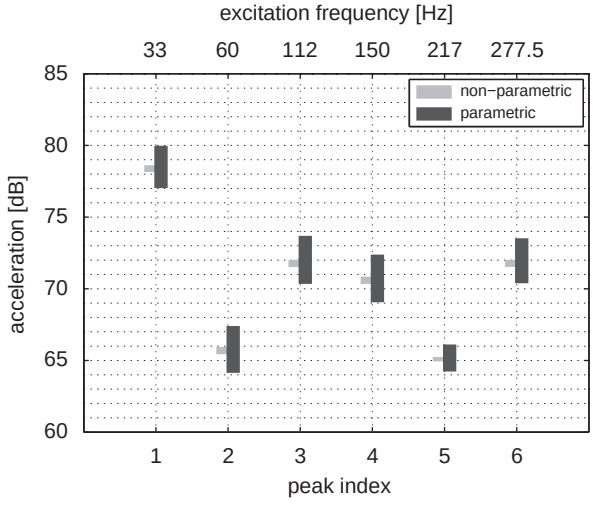

Fig. 7. Confidence region of the FRF peaks delimited by the mean value plus/minus one standard deviation, parametric and non-parametric approach; mass and stiffness deterministic.

Table 1
Comparison of the standard deviations of the FRF peaks obtained with the parametric and non-parametric approach.

Peak index	Excitation frequency (Hz)	Standard deviation (dB) (parametric)	Standard deviation (dB) (non-parametric)
1	33.0	1.4752	0.2387
2	60.0	1.6331	0.2512
3	112.0	1.6735	0.2539
4	150.0	1.6614	0.2590
5	217.0	0.9442	0.1546
6	277.5	1.5683	0.2477

peaks obtained with the non-parametric approach are in the order of about 15% of the standard deviations obtained with the parametric approach.

The shown results reveal in quantitative terms that the scatter of the FRF around the peaks obtained with the non-parametric approach is significantly smaller to that of the FRF calculated with the parametric approach. This behaviour is not fully consistent with the goal of capturing both model and parameter uncertainties, in view of the fact that the FRFs of the parametric approach, which solely takes into account parameter uncertainties, reveal a significantly higher scatter.

Based on this simple example a more complex example will be used in the next section in order to analyse the influence of the level of damping dispersion on the FRFs.

4. Case study—satellite structure

4.1. Deterministic FE model

The second analysis of the influence of the damping uncertainty in a non-parametric probabilistic model is carried out in the context of the INTEGRAL satellite of the European Space Agency (ESA) [13].

The finite element model of this structure is shown in Fig. 8 and involves approximately 120,000 DOFs. The state of the structure is assumed to remain in the linear range throughout the intended use of the model. Again, the normal mode analysis of the nominal FE model is performed using the commercial FE code MSC.Nastran [17] and the results are then imported into MATLAB [18].

The excitation consists in a harmonic support motion of the satellite in the x-direction. The support motion is implemented using the large-mass approach, i.e. by attaching an extremely large mass (greater by a factor of 10^9 than the satellite mass) and a correspondingly large excitation to the DOF at the interface between the satellite and the support. The considered response quantity is the acceleration amplitude of the tip of one of the two SAS-booms (SAS: Sun Acquisition Sensor), as marked in Fig. 8.

Damping model. In the present model, dissipation is modelled exclusively through modal damping as described in the first example (see Eq. (13)). In the nominal model, the modal damping ratios have been

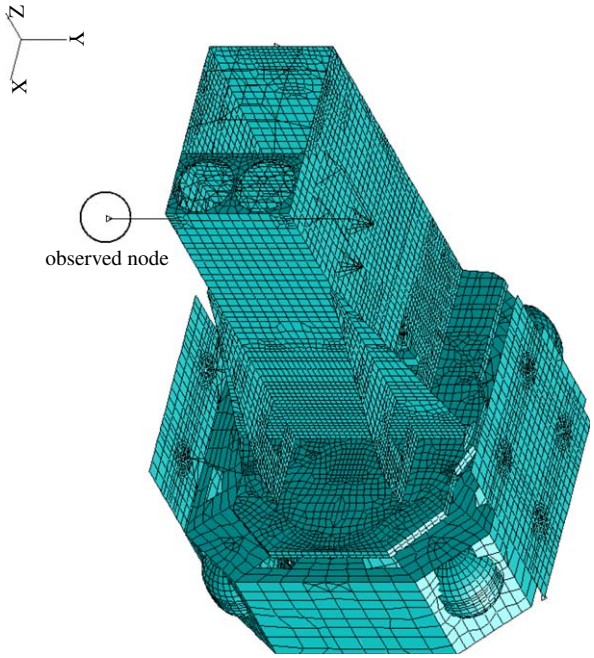

Fig. 8. Finite element model of the INTEGRAL satellite [13].

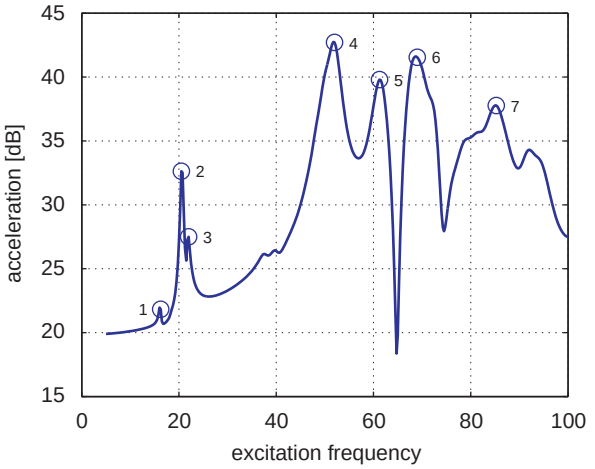

Fig. 9. Nominal structural response with numeration of peaks used for the following analysis.

assumed to take the values

$$\xi_\alpha = 1.5\% \quad \text{for } f_\alpha \leqslant 30\,\text{Hz} \quad \text{i.e. } \omega_\alpha \leqslant 188.5, \tag{14}$$

$$\xi_\alpha = 2.5\% \quad \text{for } f_\alpha > 30\,\text{Hz} \quad \text{i.e. } \omega_\alpha > 188.5. \tag{15}$$

The nominal structural response of the investigated node due to an excitation in the frequency range [5, 100] Hz is shown in Fig. 9 with the numeration of the peaks that are investigated in the following analysis.

4.2. Influence of the damping dispersion on the frequency response scatter

4.2.1. Case 1: mass and stiffness dispersion included

In Ref. [13] a non-parametric model has been constructed for the above introduced satellite FE model. The non-parametric model has been calibrated with respect to the parametric model. More specifically, calibration consists in enforcing convergence of the PDF of the first eigenfrequency of the non-parametric model to that of the parametric model. This has lead to the dispersion parameters $\delta_M = 0.1422$ for the mass matrix and $\delta_K = 0.1349$ for the stiffness matrix [13].

In order to identify the number of simulations necessary to obtain stochastic convergence for the 1%- and 99%-quantiles of the FRF peaks, a convergence analysis is carried out. The convergence is analysed studying the FRF peak quantiles, where the results of the second peak are shown in Fig. 10. The results reveal that 1000 simulations are sufficient for reliably estimating the quantiles.

In order to assess the influence of the damping dispersion parameter, δ_D, on the uncertain frequency response, the FRF ensembles of the non-parametric model have been computed for different values of δ_D. Three levels of the damping dispersion have been investigated: $\delta_D = 0\%$, 20.91% and 41.66%.

Fig. 11 depicts the confidence regions of the FRF peak responses delimited by the 1%- and 99%-quantiles. The abscissa corresponds to the peak index, with the corresponding excitation frequency f shown at the top of the figure, whereas the ordinate corresponds to the logarithm of the acceleration amplitude Y at the examined node, i.e. $20\log_{10}\|Y(\omega)\|$.

While the case of $\delta_D = 0\%$ corresponds to deterministic damping in the parametric model, in which the nominal damping ratios given by Eqs. (14) and (15) apply, the latter two levels of δ_D correspond to a parametric model in which the modal damping ratios are log-normal random variables Ξ_α, with the following mean and coefficient of variation:

$$\mathrm{E}\{\Xi_\alpha\} = \xi_\alpha, \quad \mathrm{CoV}_{\Xi_\alpha} = 0.20 \quad \text{for } \delta_D = 0.2091, \tag{16}$$

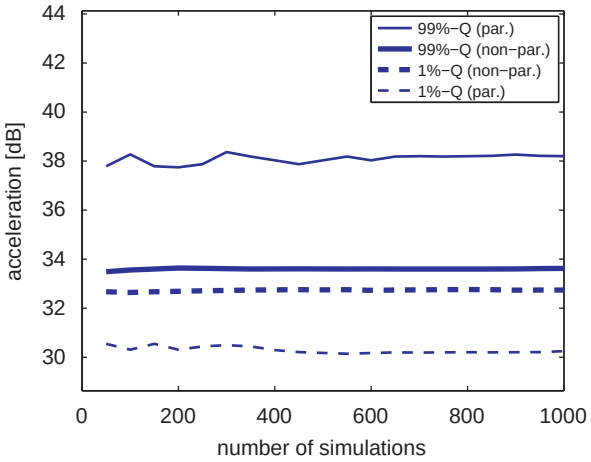

Fig. 10. Convergence analysis of the 1%- and 99%-quantiles of the second FRF peak, parametric ($\mathrm{CoV}_D = 0.20$) and non-parametric approach ($\delta_D = 0.2091$); mass and stiffness deterministic.

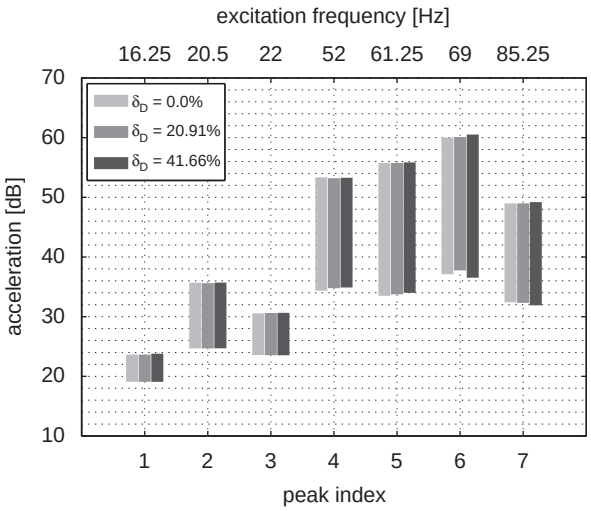

Fig. 11. Confidence region of FRF peaks delimited by the 1%- and 99%-quantiles, non-parametric approach for different levels of δ_D; mass and stiffness dispersion included ($\delta_M = 0.1422$ and $\delta_K = 0.1349$).

$$\mathrm{E}\{\Xi_\alpha\} = \xi_\alpha, \quad \mathrm{CoV}_{\Xi_\alpha} = 0.40 \quad \text{for } \delta_D = 0.4166, \tag{17}$$

where ξ_α is given by Eqs. (14) and (15).

As one can observe in Fig. 11, the three confidence regions corresponding to very different levels of the dispersion parameter δ_D are almost unchanged at the respective peak, as the maximum difference of the limits is less than 1 dB for peak 6. This indicates the insensitivity of the FRF dispersion with respect to the damping dispersion in the presence of mass and stiffness uncertainty (dispersion).

4.2.2. Case 2: mass and stiffness deterministic

Fig. 12 shows the influence of δ_D on the FRF quantiles if the mass and the stiffness properties (and hence the corresponding matrices) are deterministic, i.e. if $\delta_M = \delta_K = 0$. In comparison to Fig. 11, the three bars of the respective level of the damping dispersion differ remarkably in the upper frequency band, more specifically in the range [50,100] Hz. In contrast, in the lower frequency range the differences between the various levels of δ_D are still negligible. In other words, one can observe in this figure that in the low frequency range, namely

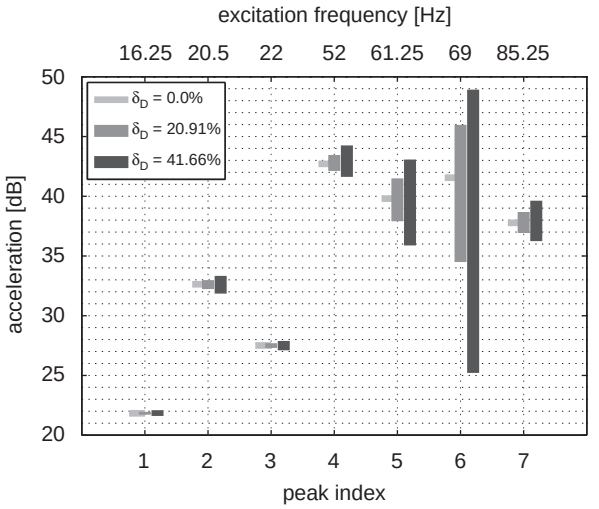

Fig. 12. Confidence region of FRF peaks delimited by the 1%- and 99%-quantiles, non-parametric approach for different levels of δ_D; mass and stiffness deterministic ($\delta_M = \delta_K = 0.0$).

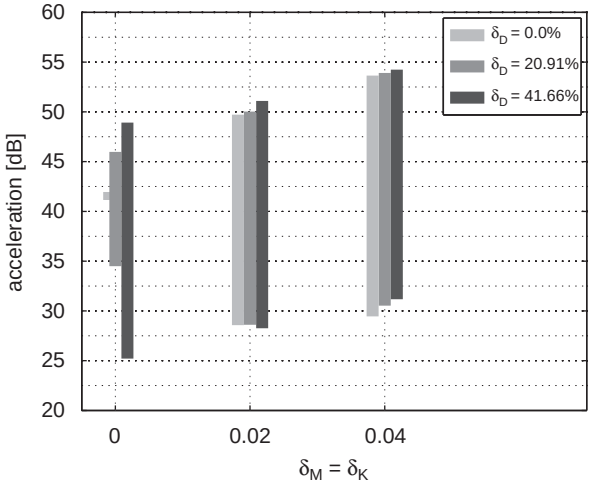

Fig. 13. Confidence region of FRF peak no. 6 delimited by the 1%- and 99%-quantiles, non-parametric approach for different levels of δ_D with varying mass and stiffness dispersion.

[5,35] Hz, the influence of the damping dispersion parameter is negligible even if the mass and stiffness matrices are deterministic.

4.2.3. Case 3: mass and stiffness dispersion gradually increasing

Next, the influence of different levels of δ_D on the FRF quantiles is considered if the dispersion parameters δ_M and δ_K are gradually increased. Fig. 13 depicts the confidence regions of the FRF at peak no. 6 (see Fig. 9) for three different cases, namely $\delta_M = \delta_K = 0.0$, $\delta_M = \delta_K = 0.02$ and $\delta_M = \delta_K = 0.04$. It is shown that even a moderate dispersion in the mass and the stiffness (controlled by the parameters δ_M, δ_K) has the effect that the influence of δ_D on the FRF quantiles is negligible. More specifically, for dispersion parameters δ_M, δ_K equal to 0.02, one can still observe a perceptible influence of the damping dispersion. In contrast, for a value of δ_M, δ_K of 0.04, the sensitivity of the FRF quantiles to δ_D has vanished entirely. These results indicate the significantly

higher sensitivity of the FRF scatter to the dispersion of the mass and the stiffness, than to the dispersion of the damping.

4.3. Influence of the damping dispersion parameter in models with higher nominal damping

As the influence of δ_D on the FRF quantiles can be expected to depend on the nominal (mean) value of the damping, in the present section the influence of the nominal damping is studied. As mentioned in Section 4.1, the dissipation is modelled exclusively by modal damping, with the nominal damping ratios specified according to Eqs. (14) and (15).

A parameter study has been conducted, in which the nominal values of the modal damping ratio have been assigned successively the values $\xi_{\text{nom}} = 0.01, 0.05, 0.10$ and 0.20. The dispersion parameters of the mass and the stiffness matrix have been assigned the fixed values of $\delta_M = 0.1422$ and $\delta_K = 0.1349$.

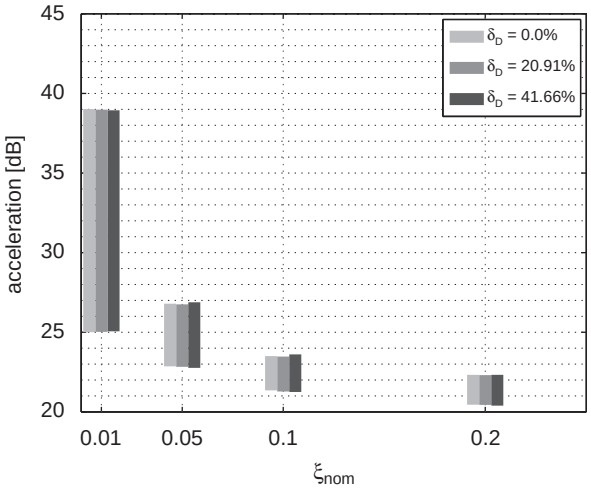

Fig. 14. Confidence region of FRF peak no. 2 delimited by the 1%- and 99%-quantiles, non-parametric approach for different levels of δ_D with varying nominal damping ratio ξ_{nom}.

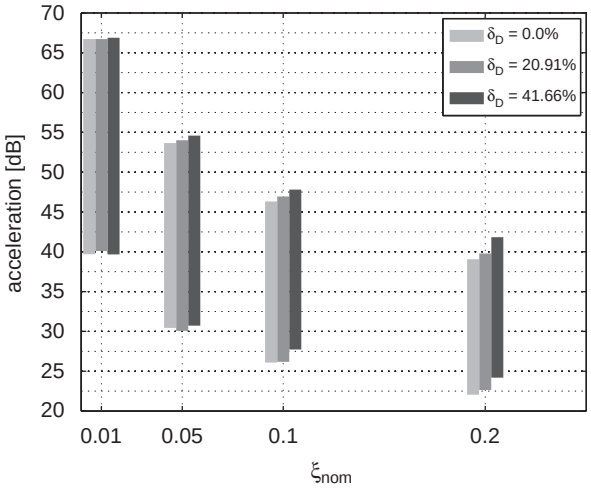

Fig. 15. Confidence region of FRF peak no. 6 delimited by the 1%- and 99%-quantiles, non-parametric approach for different levels of δ_D with varying nominal damping ratio ξ_{nom}.

The corresponding results are shown in Figs. 14 and 15, where the confidence regions of the FRF peak nos. 2 and 6, respectively, are depicted. The figures indicate that with increasing nominal damping ratios, the influence of the damping dispersion parameter on the magnitude of the scatter in the FRF does not change considerably.

However, it can be noted that with increasing magnitude of ξ_{nom} the value of δ_D does have an effect on the quantiles, in that for increasing δ_D the confidence region slightly shifts upwards. Fig. 16 confirms this trend by showing the 1%-, 50%-quantiles and 99%-quantiles over the entire frequency range. For a given value of δ_D the different quantiles can be identified by considering that—by definition—the lowest (highest) line corresponds to the lowest (highest) quantile. As the figure indicates, in the frequency band above 60 Hz (which includes peak 6) the quantiles corresponding to a given probability level are shifted upwards, as δ_D increases.

4.4. Comparison of the influence of damping dispersion in the non-parametric and the parametric model

The observations gathered in the previous sections revealed a remarkable insensitivity of the FRFs of the non-parametric model in the low-frequency domain, with respect to the level of the damping dispersion. This behaviour greatly differs from that observed in the context of parametric models of uncertainties in structural dynamics.

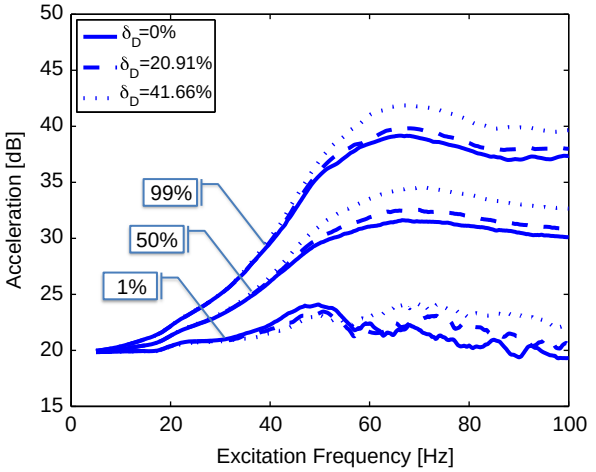

Fig. 16. FRF quantiles (1%, 50%, 99%) for different levels of δ_D; nominal damping ratio $\xi_{\text{nom}} = 0.20$; $\delta_M = 0.1422$, $\delta_K = 0.1349$.

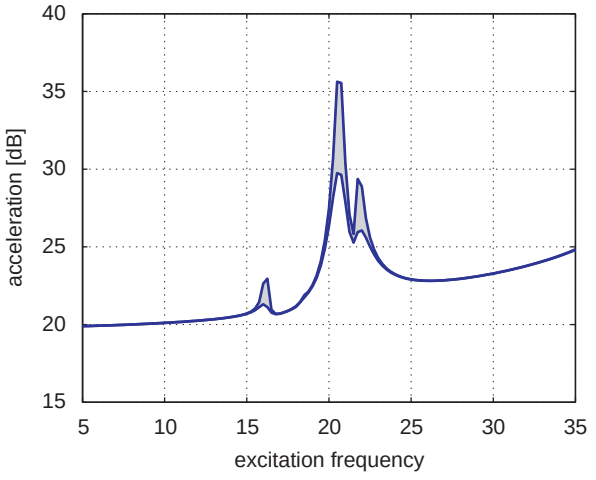

Fig. 17. Confidence region of FRF in low frequency range $f = [5, 35]$ Hz, delimited by the 1%- and 99%-quantiles, parametric approach; mass and stiffness deterministic.

Indeed, in such models the FRFs are known to be very sensitive to the level of damping scatter in the low frequency domain. To emphasize that this difference between the parametric and the non-parametric model is also very pronounced in the present case study, Figs. 17 and 18 show the confidence regions of the structural response of the parametric and non-parametric approach, for the case in which the mass and the stiffness matrices are deterministic. A direct comparison of the FRF peak quantiles of the parametric model and the non-parametric

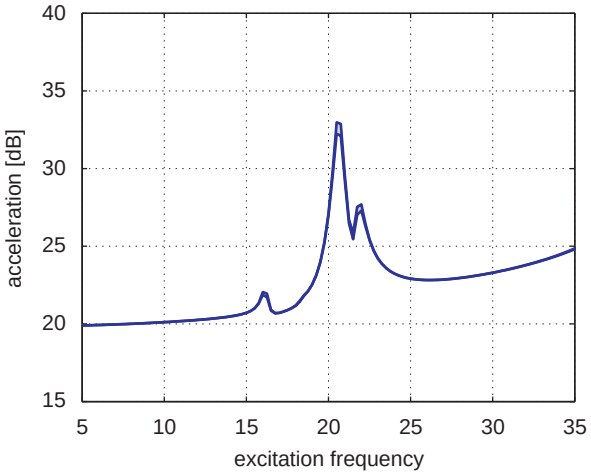

Fig. 18. Confidence region of FRF in low frequency range $f = [5, 35]$ Hz, delimited by the 1%- and 99%-quantiles, non-parametric approach; mass and stiffness deterministic.

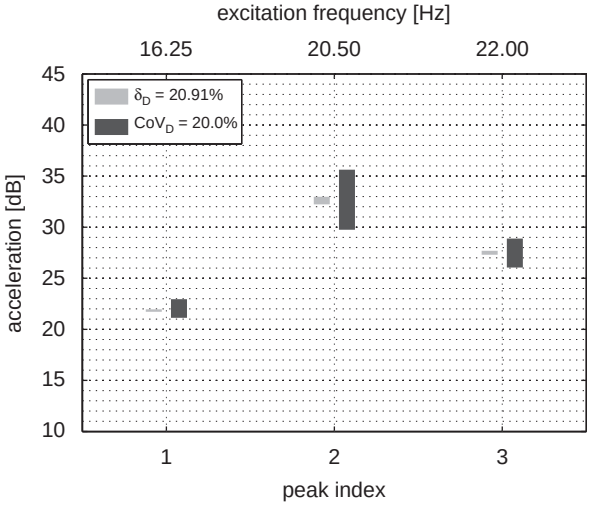

Fig. 19. Confidence region of the first three FRF peaks, delimited by the 1%- and 99%-FRF quantiles, non-parametric (δ_D) and parametric (CoV_D) approach; mass and stiffness deterministic.

Table 2
Comparison of the standard deviations of the first three FRF peaks, parametric and non-parametric approach.

Peak index	Excitation frequency (Hz)	Standard deviation (dB) (parametric)	Standard deviation (dB) (non-parametric)
1	16.25	0.5955	0.0778
2	20.50	6.6154	0.7982
3	22.00	1.6798	0.2301

model is carried out in Fig. 19, where the confidence regions defined by the 1%- and 99%-quantiles of the first three FRF peaks are depicted. The comparison of the standard deviations is listed in Table 2.

In the parametric model, the uncertainty in the damping is accounted for by modelling the modal damping ratios as log-normal random variables with a CoV of 20%, i.e. according to Eq. (16). The damping dispersion parameter of the used non-parametric model, $\delta_D = 0.2091$, corresponds to that obtained with Eq. (8), i.e. using the calibration method proposed in Ref. [13]. It should be noted that in Fig. 19 CoV_D denotes the coefficient of variation of the modal damping ratios and corresponds to $\mathrm{CoV}_{\Xi_\alpha}$ in Eqs. (16) and (17).

The above referenced results show in quantitative terms that the non-parametric model exhibits a strongly reduced scatter in comparison to the parametric model used for its calibration.

Impact of different choices for the PDF of the modal damping ratios. In the following, the question is addressed whether the choice of the PDF of the damping ratios in the parametric model influences the FRF variability in a significant way. If this was the case, one could conclude that the significant difference of the sensitivity of the non-parametric and the parametric model w.r.t. damping dispersion is contingent on a particular distribution model for the modal damping ratios in the parametric model.

The considered distributions of the modal damping ratios are shown in Fig. 20 for the case in which $\mathrm{CoV}_{\Xi_\alpha} = 0.20$ and $f_\alpha \leqslant 30$ Hz (cf. Eqs. (14) and (16), respectively). Four different assumptions for the PDF of the modal damping ratios in the parametric model have been considered: log-normal, correlated log-normal, truncated-Gaussian and Gamma-distributed. An exponential correlation model has been used in the case of the correlated log-normal PDF, with the form

$$\rho(\alpha, \beta) = \exp(-0.05|\alpha - \beta|), \tag{18}$$

where ρ denotes the correlation coefficient and α and β are the indices of the corresponding diagonal damping entries (Fig. 21).

The mass and stiffness matrices have been assumed to be deterministic throughout Figs. 22–25, that show the confidence regions of the first three FRF peaks of the parametric model in the low frequency range, where the $\mathrm{CoV}_{\Xi_\alpha}$ assumes the values of 0, 20% and 40%. As one can observe, the confidence regions of the FRFs are nearly identical in all four of the figures, showing that the choice of the PDF for the modal damping ratios is rather uninfluential. Consequently, in the sequel the originally proposed log-normal distribution is used to model the i.i.d. (independent, identically distributed) damping ratios.

4.5. Analysis of the damping matrix in the non-parametric approach

To further investigate the reasons for the limited influence of the damping dispersion parameter on the FRF in the non-parametric model, the properties of the damping matrix of the non-parametric model are analysed in this section.

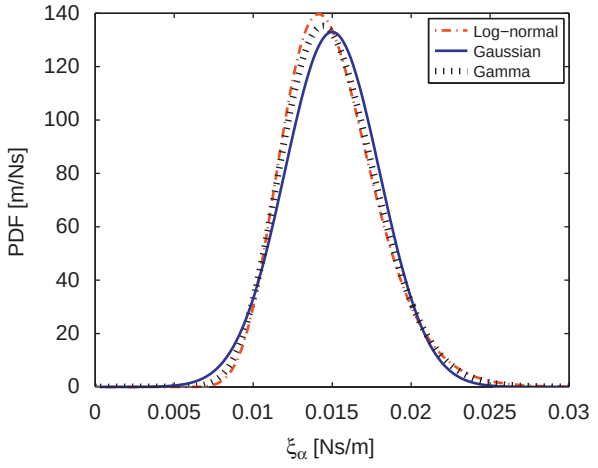

Fig. 20. Alternative probability density functions of the modal damping ratios for $f_\alpha \leqslant 30$ Hz and $\mathrm{CoV}_D = 20\%$.

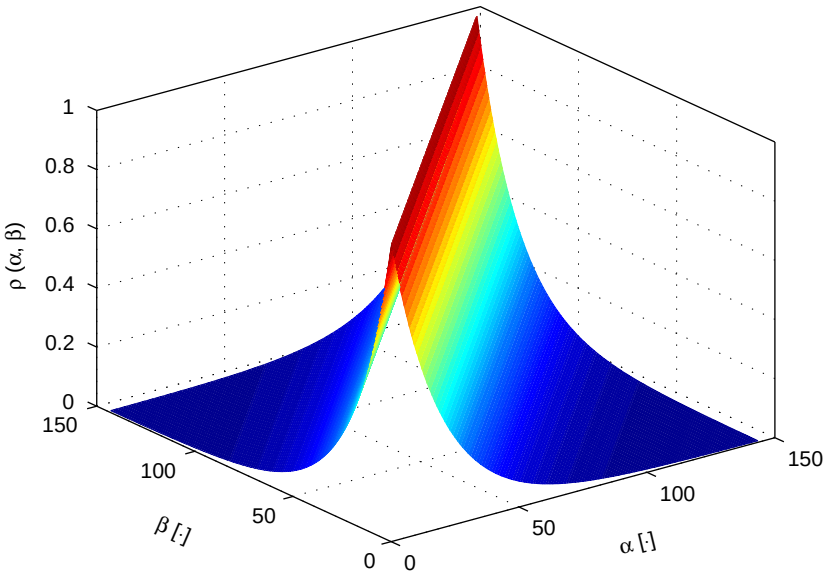

Fig. 21. Correlation model $\rho(\alpha,\beta)$ of the correlated, log-normal distributed modal damping ratios in the parametric probabilistic model.

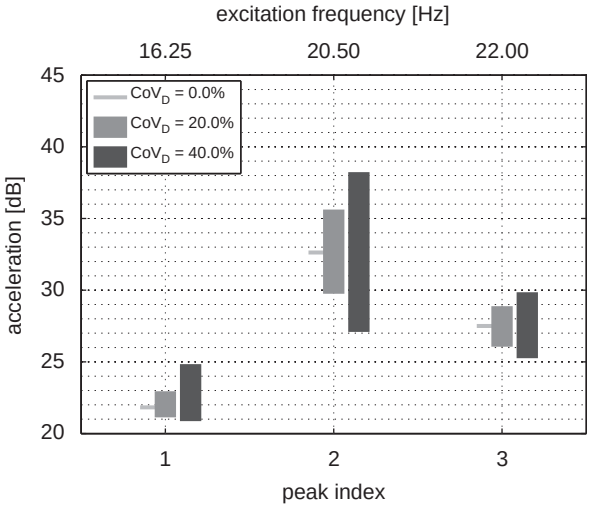

Fig. 22. Confidence region of first three FRF peaks, delimited by the 1%- and 99%-quantiles, parametric model, log-normal distributed modal damping ratios; $\mathrm{CoV}_M = \mathrm{CoV}_K = 0$.

The structure of the damping matrix in the modal space is shown in Fig. 26. In this 3D-plot ("city plot") the α- and β-axes refer to the indices of the damping matrix entries, whereas the vertical axis denotes the value of the corresponding damping matrix entry, $\mathbf{D}^{\mathrm{np}}_{\mathrm{red}\alpha\beta}$. As opposed to the reduced model in the parametric approach, the non-parametric model is characterized by full matrices in the modal space. However, Fig. 26 shows that the off-diagonal terms do not deviate considerably from zero and consequently the damping matrix is dominated by its diagonal terms. Hence, the off-diagonal terms are not considered in the following analysis of the damping matrix scatter.

Diagonal entries of the damping matrix. Next, the scatter of the diagonal components of the damping matrices is analysed. Figs. 27 and 28 depict the values of the diagonal entries of the damping matrix of the parametric and the non-parametric model, respectively, for five different random realizations (regular solid lines), as well as for the deterministic damping matrix (bold solid line). The abscissa refers to the index α of the

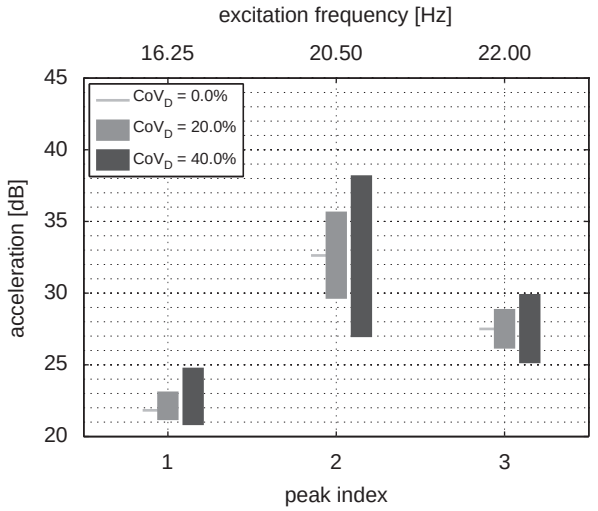

Fig. 23. Confidence region of the first three FRF peaks delimited by the 1%- and 99%-quantiles, parametric model, correlated, log-normal distributed modal damping ratios; $\mathrm{CoV}_M = \mathrm{CoV}_K = 0$.

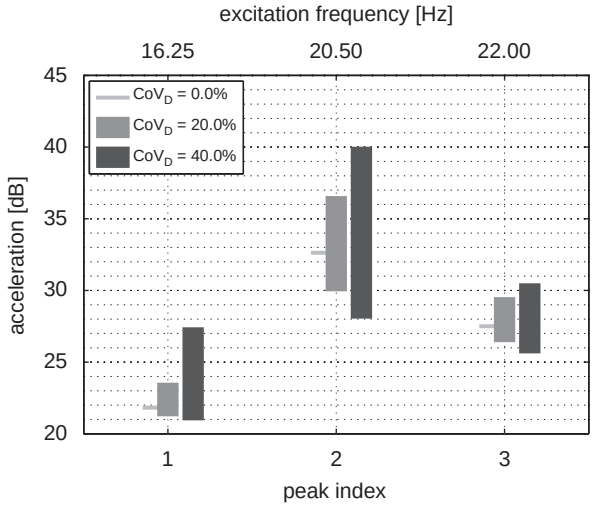

Fig. 24. Confidence region of the first three FRF peaks, delimited by the 1%- and 99%-quantiles, parametric model, truncated Gaussian distributed modal damping ratios; $\mathrm{CoV}_M = \mathrm{CoV}_K = 0$.

considered diagonal entry of the damping matrix; on the ordinate the value of the corresponding damping matrix entry, $\mathbf{D}^{\mathrm{par}}_{\mathrm{red}\alpha\alpha}$ and $\mathbf{D}^{\mathrm{np}}_{\mathrm{red}\alpha\alpha}$, respectively, is shown (cf. Eqs. (13) and (6)). The plots refer to the case in which the CoV of the damping ratios amounts to 20% (Eq. (16)). The two figures show that the diagonal damping entries of the parametric model have a remarkably higher scatter than the diagonal damping entries of the non-parametric model. Although a direct comparison of the non-parametric and parametric model is not justified due to the different types of uncertainties modelled by the two approaches, the results indicate that the scatter in the diagonal damping matrix entries is disproportionately low in the non-parametric model.

It is reasonable to expect that an increase of the damping dispersion parameter will lead to a more pronounced scatter in the diagonal damping entries of the non-parametric model, and, as a consequence, of the corresponding frequency response in the low frequency range. The next section will expand on this statement in a quantitative fashion.

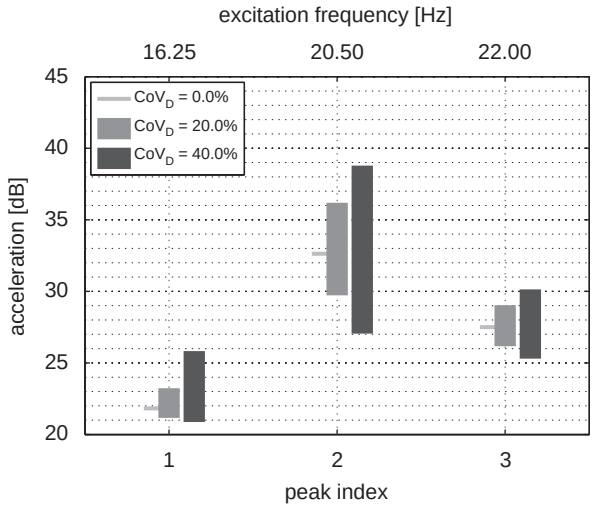

Fig. 25. Confidence region of the first three FRF peaks, delimited by the 1%- and 99%-quantiles, parametric model, Gamma distributed modal damping ratios; $\mathrm{CoV}_M = \mathrm{CoV}_K = 0$.

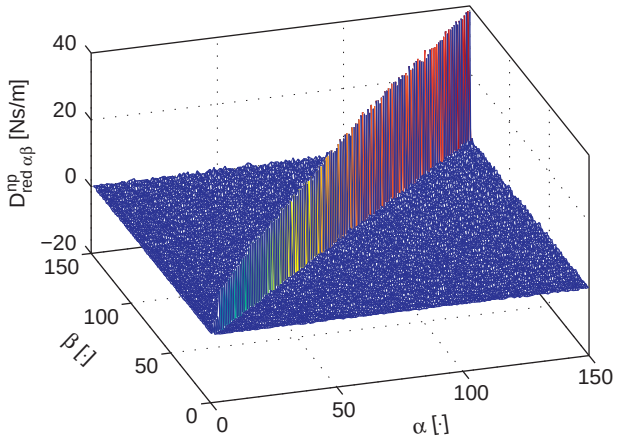

Fig. 26. City plot of the reduced damping matrix of the non-parametric model.

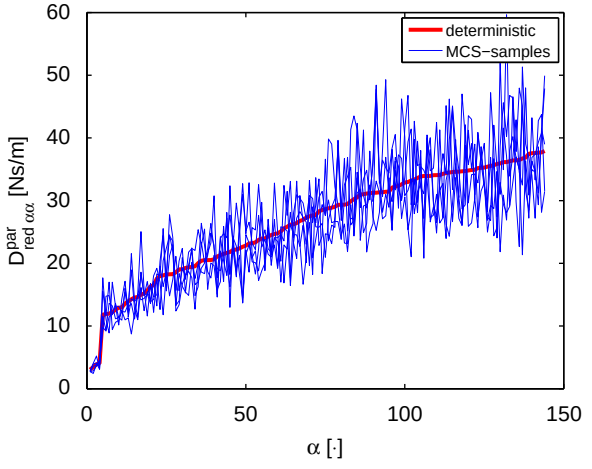

Fig. 27. Diagonal entries of the damping matrix, parametric model; deterministic case and five random realizations (MCS), $\mathrm{CoV}_D = 20\%$.

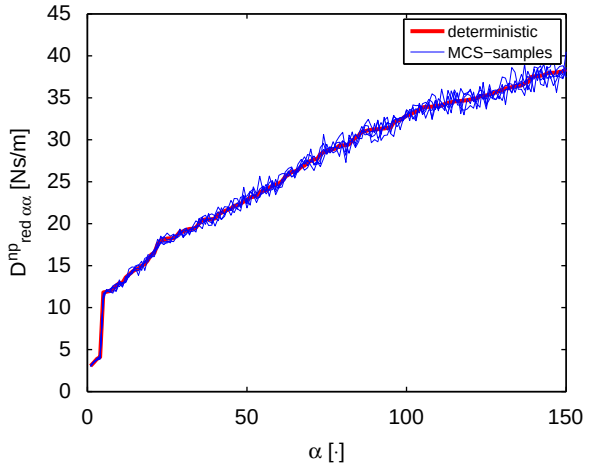

Fig. 28. Diagonal entries of the damping matrix, non-parametric model; deterministic case and five random realizations (MCS), $\delta_D = 20.91\%$.

4.6. *Alternative calibration criterion for the damping dispersion parameter*

4.6.1. *Damping matrix-based calibration*

As presented in Section 4.4, a non-parametric model, in which the damping dispersion level is determined on the basis of Eqs. (8) and (9), will exhibit a very low scatter in the FRFs due to damping variability (see Fig. 19).

Since the FRFs of real structures are expected to be significantly influenced by the damping around the first resonance frequencies, the FRFs predicted with *this* non-parametric model, in which the damping dispersion parameter has been calibrated on the basis of the damping matrices, is not deemed fully satisfactory. Hence, an alternative calibration criterion has been proposed in Section 2.4; the properties and the FRF predictions of the associated non-parametric model will be addressed in the next subsection.

4.6.2. *FRF-peak-based calibration*

The novel calibration criterion introduced in this paper enforces the correspondence of the scatter in the FRFs of the parametric and the non-parametric model, at the first eigenfrequency. For the investigated numerical model the excitation frequency is therefore set to $f = 16.208$ Hz. In this case study, a moderate scatter in the log-normally distributed modal damping ratios of the parametric model has been assumed, namely with a CoV of 10%. The damping dispersion parameter, δ_D, of the non-parametric model has then been calibrated according to Eqs. (10)–(12), where Y_1 corresponds to the acceleration amplitude of the SAS boom indicated in Fig. 8.

The implementation of this procedure, i.e. the solution of the minimization problem in Eq. (12), has made use of the MATLAB-function `fminsearch` [18], which finds the minimum of a function using the Nelder–Mead simplex method. The termination tolerance on the function value, i.e. for $J(\delta_D)$, has been set to 10^{-4}, the tolerance on the parameter δ_D, has been set to 10^{-3}.

After 25 iteration steps the damping dispersion parameter converged to $\delta_D = 0.81125$. Clearly, the obtained value for δ_D is significantly larger than the one obtained with the calibration criterion based on the damping matrix, which leads to $\delta_D \approx 10\%$.

The histograms of the acceleration FRF of the parametric and the non-parametric model, at $f = 16.208$ Hz, are shown in Fig. 29. As confirmed by the graphs in the figure, the non-parametric model with $\delta_D = 0.81125$ results in an FRF scatter at the first eigenfrequency, which closely matches that of the parametric model.

To further validate the alternative calibration method, the FRF quantiles obtained with the parametric model ($\mathrm{CoV}_{\Xi_\alpha} = 0.10$) and with the resulting non-parametric model ($\delta_D = 0.81125$) are compared directly in the lower frequency band, i.e. in the range of [5,35] Hz (Fig. 30) by means of the confidence regions defined by the 1%- and 99%-quantile of the first three FRF peaks. Clearly, the confidence regions of the parametric and

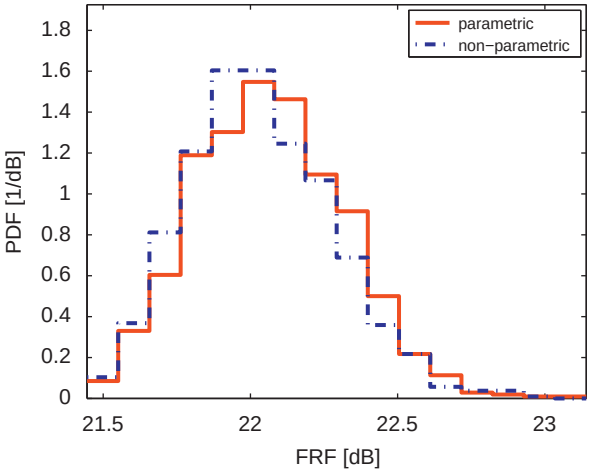

Fig. 29. Approximate probability distribution functions of the FRF at the first eigenfrequency.

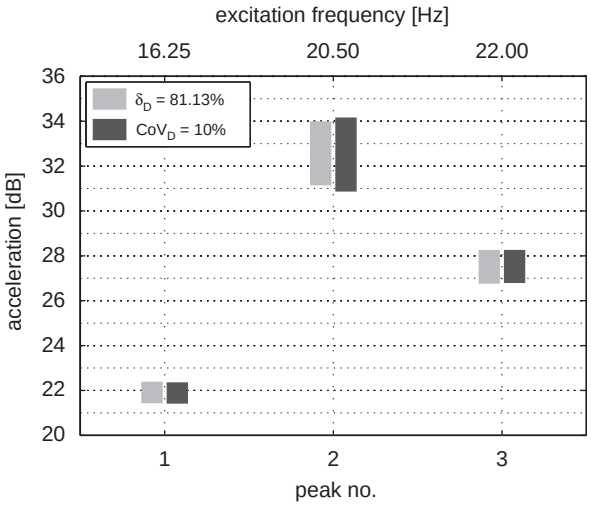

Fig. 30. Confidence region of the first three FRF peaks, delimited by the 1%- and 99%-quantiles, parametric and non-parametric model; mass and stiffness deterministic ($CoV_M = CoV_K = 0$).

the non-parametric model match reasonably well. It should be noted that this correspondence is obvious for the first eigenfrequency, since this very correspondence represents the convergence criterion. However, the good agreement carries over also to the next-higher eigenfrequencies.

5. Conclusions

In the present paper the role of the damping dispersion parameter in the adopted non-parametric model of uncertainties in structural dynamics has been investigated. It has been shown that in this non-parametric model the influence of the damping dispersion on the scatter in the FRF is relatively small, if the calibration criterion based on the damping matrix norm is used.

A novel method for calibrating the non-parametric model has been proposed, which enforces the same scatter of the FRF at the first resonance frequency, in the parametric and the non-parametric model, respectively. The present case study shows that with this approach for the calibration, the FRF scatter of the non-parametric model, around the resonance frequencies in the low frequency range, reaches a level similar to

that of the parametric model used for its calibration. Since in a model with deterministic mass and stiffness properties, as used here, the FRF scatter is exclusively due to the scatter in the damping, this correspondence is deemed as a suitable indicator for the appropriate level of the damping dispersion parameter in the non-parametric model.

Acknowledgements

The authors thank the European Space Research and Technology Center (ESTEC) of the European Space Agency (ESA) for providing the satellite FE model. The partial financial support by the AMADEUS European program (Project no. 22/2003 and LAM03), as well as the support of the Frankreich-Schwerpunkt at the LFU Innsbruck, are gratefully acknowledged. The support of Prof. Schuëller, as well as the helpful comments by Prof. Soize and Dr. Capiez-Lernout are greatly appreciated and acknowledged.

The first author is a recipient of a DOC-fForte-fellowship of the Austrian Academy of Science at the Institute of Engineering Mechanics (University of Innsbruck).

References

[1] C. Soize, A comprehensive overview of a non-parametric probabilistic approach of model uncertainties for predictive models in structural dynamics, *Journal of Sound and Vibration* 288 (3) (2005) 623–652.
[2] G. Schuëller, On the treatment of uncertainties in structural mechanics and analysis, *Computers and Structures* 85 (5–6) (2007) 235–243.
[3] R. Singh, C. Lee, Frequency response of linear systems with parameter uncertainties, *Journal of Sound and Vibration* 168 (1993) 71–92.
[4] C. Papadimitriou, L. Katafygiotis, J. Beck, Approximate analysis of response variability of uncertain linear systems, *Probabilistic Engineering Mechanics* 10 (1995) 251–264.
[5] C. Bucher, C. Brenner, Stochastic response of uncertain systems, *Archive of Applied Mechanics* 62 (1992) 507–516.
[6] R. Menezes, G. Schuëller, On structural reliability assessment considering mechanical model uncertainties, in: H.G. Natke, Y. Ben-Haim (Eds.), *Uncertainty*: *Models and Measures*: *Proceedings of the International Workshop*, Vol. 1, Lambrecht, Germany, July 22–24, 1996, Akademie Verlag, Berlin, 1996, pp. 175–186.
[7] H. Chebli, C. Soize, Experimental validation of a nonparametric probabilistic model of nonhomogeneous uncertainties for dynamical systems, *Journal of the Acoustical Society of America* 115 (2) (2004) 697–705.
[8] T. Paez, J. Red-Horse, Structural dynamics challenge problem: summary, *Computer Methods in Applied Mechanics and Engineering* 197 (29–32) (2008) 2660–2665.
[9] C. Soize, A nonparametric model of random uncertainties for reduced matrix models in structural dynamics, *Probabilistic Engineering Mechanics* 15 (2000) 277–294.
[10] C. Soize, Nonlinear dynamical systems with nonparametric model of random uncertainties, *Uncertainties in Engineering Mechanics* 1 (2001) 1–38.
[11] C. Soize, Maximum entropy approach for modeling random uncertainties in transient elastodynamics, *Journal of the Acoustical Society of America* 109 (2001) 1979–1996.
[12] M.F. Pellissetti, E. Capiez-Lernout, H.J. Pradlwarter, C. Soize, G.I. Schuëller, Reliability analysis of large scale structures using a non-parametric approach, *Computer Methods in Applied Mechanics and Engineering* 198 (2) (2008) 334–357.
[13] E. Capiez-Lernout, M. Pellissetti, H. Pradlwarter, G. Schuëller, C. Soize, Data and model uncertainties in complex aerospace engineering systems, *Journal of Sound and Vibration* 295 (3–5) (2006) 923–938.
[14] E. Capiez-Lernout, C. Soize, Nonparametric modeling of random uncertainties for dynamic response of mistuned bladed disks, *Journal of Engineering for Gas Turbines and Power—Transactions of the ASME* 126 (2004) 610–618.
[15] M. Arnst, D. Clouteau, M. Bonnet, Inversion of probabilistic structural models using measured transfer functions, *Computer Methods in Applied Mechanics and Engineering* 197 (6–8) (2008) 589–608.
[16] R. Cottereau, D. Clouteau, C. Soize, Construction of a probabilistic model for impedance matrices, *Computer Methods in Applied Mechanics and Engineering* 196 (2007) 2252–2268.
[17] MSC.NASTRAN, Version 70.7, MSC.Software Corporation, 2001.
[18] Matlab R2006b, The MathWorks, Natick, MA, USA, 2006.